Interfacial Layering in a Three-Component Polymer System

A. Aradian,*,†,‡ F. Saulnier,† E. Raphaël,† and P.-G. de Gennes†

Physique de la Matière Condensée, C.N.R.S. UMR 7125 & Fédération de Recherche MSC (FR 2438), Collège de France, 11 place Marcelin Berthelot, 75231 Paris Cedex 05, France, and University of Edinburgh, School of Physics, King's Buildings JCMB, Edinburgh EH9 3JZ, United Kingdom

Received October 23, 2003; Revised Manuscript Received April 5, 2004

ABSTRACT: We study theoretically the temporal evolution and the spatial structure of the interface between two polymer melts involving *three* different species (A, A*, and B). The first melt is composed of two different polymer species A and A* which are fairly indifferent to one another (Flory parameter $\chi_{AA} \simeq 0$). The second melt is made of a pure polymer B which is strongly attracted to species A ($\chi_{AB} < 0$) but strongly repelled by species A* ($\chi_{A^*B} > 0$). We then show that, due to these contradictory tendencies, interesting properties arise during the evolution of the interface after the melts are put into contact: as diffusion proceeds, the interface structures into several adjacent "compartments", or layers, of differing chemical compositions, and in addition, the central mixing layer grows in a very asymmetric fashion. Such unusual behavior might lead to interesting mechanical properties and demonstrates in a specific case the potential richness of multicomponent polymer interfaces (as compared to conventional two-component interfaces) for various applications.

1. Introduction and Motivation

The phenomena taking place at the interfaces and surfaces of polymeric systems are obviously of high importance to many practical or industrial situations. As a result, they have been the focus of extensive study both experimentally and theoretically in the recent decades. Much progress has been made in the understanding of these phenomena as well as in the development of techniques to characterize them (see e.g. the general refs 1−4).

1.1. Interfaces between Polymer Melts. One situation that has received much attention is that of two pieces of molten polymer put into (good) contact at a certain initial time: how does then the interface between these melts evolve, and how does the mixing between the melts occur, if any; or, more precisely, what is the final, equilibrium state reached by the system (i.e., given enough time, does it mix fully or only in a restricted region?), and with what kind of concentration profile? What is the dynamics leading to that final state, over which typical time scales? It has been found,[1,2] due to the specific physics of polymer macromolecules, that their mixing is generally quite different from what is known in more conventional diffusive systems, like molecular gases.

Once the two polymer pieces are put into contact, the subsequent evolution will obviously generally depend on the various physicochemical properties of the materials facing each other (nature of microscopic interactions between monomers, chain length, topological structure, etc.). It has been recognized however that, at least from a conceptual standpoint, the two most crucial parameters determining the fate of the system are the sign and magnitude of the product χN, where χ is the Flory parameter,[5] related to the microscopic interactions between components, and N is the chain length. We will remind of the different possibilities for χN in section 2.

1.2. Multicomponent Interfaces. To facilitate the identification and modeling of the fundamental processes at work within polymer/polymer interfaces, past studies have for the most part, if not exclusively, focused on interfaces involving *two* species (for instance, one on each side of the interface) and sometimes only one species (interfaces between two identical melts). Certainly, the span of real situations is much wider, with a vast range of multicomponent interfaces, and one is thus entitled to ask what is the structure and dynamics of an interface between two polymer mixtures involving more than two components.

As exemplified in the case studied in this article, such multicomponent interfaces may have an interest of their own, as a means (for example) of obtaining structured interfaces at a submicron scale: when two polymer mixtures are put into contact, and provided the contrast in relative miscibilities of the different components is adequate, a "multiple" interface may form; that is to say, the interface will partition into several adjacent layers, each of different chemical composition. A possible application of this could be the formation of multilayer polymer films. The mechanical properties presented by the resulting assembly might also prove interesting.

Multispecies interfaces can also appear in the course of an interfacial reaction between two polymers: when the polymer pieces are put into contact, a reaction may start at the interface that delivers a (polymer) product whose miscibilities with each of the initial reactants are different; this three-species system is susceptible to lead to a multiple interface, whose dynamics is then coupled to that of the chemical reaction.

However, on purely combinatorial grounds, the diversity of all conceivable multicomponent interfaces makes any general approach likely to be hopeless; thus, delineating and focusing on a certain number of limiting situations may be useful. This is indeed the purpose of the present article: we will be considering one such "selected case" for a three-component interface and will show that it exhibits a peculiar spatial structure and evolution through time, which we will fully analyze.

The article is organized as follows: in section 2, we start with a reminder on the standard theoretical results concerning two-component interfaces, as these

† Collège de France.
‡ University of Edinburgh.
* Corresponding author. E-mail A.Aradian@ed.ac.uk.

10.1021/ma0356008 CCC: $27.50
Published on Web 05/14/2004

will be used as basic tools for the rest of the paper. In section 3, we present the system that will be studied and try to qualitatively explain the structure of the multiple interface which appears. In section 4, we write the equations governing the system and solve them, thus finding the length scales and concentration profiles which characterize the dynamics of our system (note that, if interested only in results, our reader can skip directly to section 4.3). Section 5 closes the article with some concluding remarks.

2. A Short Overview of Two-Component Interfaces

We start here by a general overview of the standard theories describing two-species interfaces. By no means do we aim here at an exhaustive survey of the theoretical or experimental literature on the subject: we simply quickly recall the most basic theoretical elements on which our present work builds.

Let us denote the two polymer species we consider as A and B. We will cover interfaces occurring between an A-melt facing a B-melt as well as between two A−B blends facing each other but of differing A/B proportions. We will also mainly put the emphasis on the effect of varying the Flory parameter χ_{AB} between A and B, with the assumption that both A and B have the same chain length N. Situations where N_A and N_B differ (e.g., a melt of long chains facing a melt of short chains), which are still subject to some debate, will merely be hinted at.

It is a remarkable point that the kinetics of formation of interfaces between chemically different polymers is controlled by thermodynamic as well as kinetic factors. To take into account the driving or slowing role played by energetic parameters in diffusion processes, it is much convenient to use Flory−Huggins' derivation of the free energy (see eq 6 for the expression of the free energy f in this model and also ref 6): thinking in terms of a lattice model, the dimensionless Flory parameter χ_{AB} characterizes the enthalpy of mixing at the molecular level by comparing interactions between neighboring polymer segments of the same species (i.e., association energy ϵ_{AA} for two neighboring A segments, ϵ_{BB} for two B segments) and interactions between different species in contact (ϵ_{AB} for an A next to a B). If z denotes the coordination number in the lattice, we define

$$\chi_{AB} = \frac{z(2\epsilon_{AB} - \epsilon_{AA} - \epsilon_{BB})}{2kT} \tag{1}$$

In other words, χ_{AB} is the energy change, in units of the thermal energy kT, when a segment of A is taken from an environment of pure A and swapped with a segment of B from an environment of pure B. The Flory parameter χ_{AB} can be positive or, much more rarely, negative. If the only interactions existing between A and B are van der Waals forces, χ_{AB} shall be positive. Negative values of χ_{AB} do appear in polymer couples displaying specific chemical interactions, such as hydrogen bonds. The three following subsections briefly discuss the different possible cases ($\chi_{AB} > 0$, $\chi_{AB} = 0$, $\chi_{AB} < 0$) and their physical consequences.

2.1. Immiscible Components: $\chi_{AB} > 0$. As stated above, in the absence of specific interactions or structural similarities, the Flory parameter is positive and usually ranges from 10^{-3} to 10^{-1}. This is by far the most usual situation for polymer pairs. For polymer pairs differing only by isotopic substitution (e.g., when deuterium is substituted to hydrogen in the monomer structure), very small, positive values as low as $\chi_{AB} \simeq 10^{-4}$ can be found.[7]

In this case of positive χ_{AB}, the polymer pairs are immiscible for all but the lowest molecular weights: if $N = N_A = N_B$ is the length of both polymers A and B, it can be shown that, for a Flory parameter χ_{AB} greater than a critical value $\chi_C = 2/N \ll 1$, phase separation occurs, and we end up at equilibrium with macroscopic regions of pure A and pure B, separated by a sharp interfacial layer: no macroscopic mixing occurs.

Let us clarify the nature of this interface between the two coexisting phases by a simple scaling argument.[8] The characteristic width w of the interface can be estimated by a balance between the chain entropy (of order kT per chain), which tends to widen the interface, and the unfavorable enthalpy of mixing (of order $\chi_{AB}kT$ per segment), which tends to narrow the interface: thus, the typical length N_0 of a loop of an A-chain penetrating a B-rich region is given by $N_0\chi_{AB}kT \sim kT$, that is, $N_0 \sim 1/\chi_{AB}$. Because the loop has the form of a random statistical walk, this contour length corresponds to a (straight) penetration distance $w \sim a\sqrt{N_{max}}$ (where a is the monomer size). We finally find that the characteristic width of the interface is

$$w \sim \frac{a}{\sqrt{\chi_{AB}}} \tag{2}$$

This simple analysis is in accordance with the results obtained from a more rigorous description based on a square-gradient model of the interfacial free energy.[8] Note that the scaling analysis leading to this result is valid provided that $\chi_{AB}N \gg 1$: eq 2 then predicts the mixing region to be much smaller than the polymer coil size, and thus, at the macroscopic scale, the interface is to be considered as a very sharp one, with a steep profile. This property of interfaces between immiscible melts will be used thereafter in our solution (cf. section 3.2).

2.2. Entropy-Driven Mixing: $\chi_{AB} = 0$. We now consider the case of a zero Flory parameter. Rigorously speaking, this situation arises when the two polymers put into contact are identical (same chemical structure). But it is also a useful approximation to describe mixing in systems with a very small χ_{AB}, be it positive or negative (typically when $|\chi_{AB}| \ll 1/N$).

Starting from the initial situation where two polymer pieces are put into contact, the final, equilibrium state reached by the system is a homogeneous one (the initial interface has totally disappeared) with complete mixing of the polymer components. As there is no enthalpy gain associated with mixing species ($\chi_{AB} = 0$), the evolution of the system is driven solely by gains in the translational entropy of the polymer chains.

The dynamics toward this final state can be complex, especially for entangled polymers where several regimes of non-Fickean diffusion successively appear. In these entangled polymers, the first stages of the interdiffusion process between melts of equal molecular weight have been described first within a scaling approach in ref 10 and then detailed by different authors:[11−14] the chains are initially segregated on each side of the contact plane, with discontinuous concentration profiles abruptly dropping from unity to zero at the separation. Then, as the chains start interpenetrating to form a mixed layer, and because of the specific reptational dynamics of the

polymer chains, this initial discontinuity survives, with a progressively resorbing amplitude, until disappearing when the reptation time T_{rep} is reached. The interface is then said to have "healed" completely. This feature stands in obvious contrast with conventional mixing where initial discontinuities are immediately smoothed out by the diffusion process.

For times greater than the reptation time ($t > T_{rep}$), the interdiffusion dynamics becomes purely Fickean and is described by the classical diffusion equation

$$\dot{\phi} = D_s \nabla^2 \phi \tag{3}$$

The diffusion coefficient D_s, known as the "self-diffusion" coefficient, is independent of concentration and for long, entangled chains (N greater than the entanglement threshold N_e) is equal to

$$D_s = \Lambda_0 \frac{N_e}{N^2} kT \tag{4}$$

where Λ_0 is the monomeric mobility.

The use of eq 3 is valid only for facing melts with chains A and B of equal length (symmetric interfaces with $N_A = N_B$). The case of asymmetric polymer junctions, between chemically identical melts of different molecular weights (typically a melt of short chains in contact with a melt of much longer chains), proves much more subtle. The evolution of such a system also displays several temporal regimes and can essentially be understood as follows:[15,16] the long and less mobile chains behave like a gel which is progressively penetrated and swollen by the smaller species, but as the gel of long chains swells, it effectively drags the smaller chains within it. The global diffusion profile is thus rather complex and results from the microscopic diffusion of the small chains relative to the matrix of longer chains, combined with the global motion of this matrix. This global flow of the matrix, known as a "bulk flow",[9] is essential for a correct description of the system and will reappear in the next section devoted to enthalpy-driven species.

2.3 Enthalpy-Driven Mixing: $\chi_{AB} < 0$. Let us now consider the case of mixing between species driven by a gain in enthalpy, i.e., when $\chi_{AB} < 0$. A few dozens of A/B pairs with $\chi_{AB} < 0$ have been reported, like PS/PVME (polystyrene/poly(vinyl methyl ether))[17] or PVC/PMMA (poly(vinyl chloride)/poly(methyl methacrylate)). Within the temperature range where χ_{AB} remains negative, such polymer couples are fully miscible for all molecular weights.

The dynamics of "enthalpy-driven" mixing at interfaces between polymers has been the focus of many studies in the past 20 years, and its theoretical description has led to some controversy in the case where the system is asymmetric, e.g., when the mobility of the A and B chains are different (due to different chain lengths).

On the basis of Onsager's formalism of linear irreversible thermodynamics,[18,19] two main approaches were proposed.

The so-called "slow-mode" theory propounded by Brochard and co-workers[20,21] assumes that the flux of species A is the opposite of the flux of B, i.e., $J_A = -J_B$. In cases where the system is asymmetric, this hypothesis of cancellation of fluxes leads to a mutual diffusion coefficient dominated by the mobility of the slowest species—hence the name of the theory.

On the other hand, Kramer and co-workers[22] explicitly introduce a third species in their model, which play the role of vacancies in the system and move about in order to allow the motion of A and B chains. Then the fluxes of the A and B components need not be equal anymore, and their difference $J_A - J_B$ is compensated by a net flux of vacancies J_V across the cell.[23] It is furthermore postulated that the chemical potential of the vacancies is constant throughout the system, and this, contrary to the theory of Brochard et al., leads to a "fast-mode" diffusion coefficient, i.e., dominated by the fastest species in asymmetric systems.

In the recent years, several authors have tried to bridge the gap between these "slow" and "fast" theories; see for instance refs 24 and 25 and references therein.

Experimental data seem to validate the fast-mode theory.[26−30] Nonetheless, to this day, the origin and physical interpretation of the vacancy flux used in the model of Kramer et al. or in more recent approaches remain somewhat obscure. Therefore, it is conceptually most interesting to note that, in an amended version of her model,[31] Brochard showed that fast-mode predictions could be retrieved without resorting to any flux of vacancies.[32] Instead, Brochard's corrected approach shows that, in addition to the individual diffusion fluxes of A and B, there exists a global, collective motion involving both A and B; when this is taken into account, fast-mode results are found without the need of vacancies. The occurrence of such collective "bulk flows" (as they are called), superimposed to pure diffusion, is indeed known as a common feature of asymmetric diffusive systems.[9] In the amended model of Brochard, each chain of polymer reptates and diffuses within a matrix composed of all the other chains; physically, a bulk flow occurs because this matrix itself is set into motion, due to the difference of mobility between the two diffusing species (in other words, polymer chains reptate in tubes which are themselves moving).

To describe the interdiffusion process of these two different polymers, one usually employs the so-called "mutual diffusion" coefficient D_M, which relates the total flux J_i of species i (i = A or B) to the gradient of its volume fraction ϕ_i: $J_i = -D_M \nabla \phi_i$. Let us denote $\phi \equiv \phi_A = 1 - \phi_B$ the volume fraction of species A. In all the theoretical models mentioned above, the mutual diffusion coefficient can then be cast into the generic form

$$D_M = \Lambda[\phi]\phi(1-\phi)\frac{d^2 f}{d\phi^2} \tag{5}$$

where $\Lambda[\phi]$ is a positive function of ϕ (homogeneous to a mobility), which differs from model to model, and f is the classical Flory−Huggins free energy per site,[6] given by

$$\frac{f}{kT} = \frac{\phi}{N_A}\log\phi + \frac{1-\phi}{N_B}\log(1-\phi) + \chi_{AB}\phi(1-\phi) \tag{6}$$

In the rest of this article, we will only be concerned with the *symmetric* case, i.e., with polymer components of the same chain length ($N_A = N_B \equiv N$) and the same monomeric mobility Λ_0. It should be pointed out that, in this case, the conceptual subtleties mentioned above do not intervene, and interdiffusion models do agree on the same expression of the diffusion coefficient. For long,

entangled chains ($N > N_e$, the regime of interest to us), and using the same notations as in eq 4, one has simply $\Lambda = \Lambda_0 N_e/N$. From eq 5, the mutual diffusion coefficient then reads[20−22]

$$D_M = \Lambda_0 \frac{N_e}{N} kT\phi(1-\phi)\left[\frac{1}{\phi(1-\phi)N} - 2\chi_{AB}\right] \quad (7)$$

A useful limit in practice is $|\chi_{AB}|N \gg 1$: as long as ϕ and $1 - \phi$ are larger than the (small) value $\phi_c = 1/(2|\chi_{AB}|N)$, D_M can be approximated as

$$D_M = D_f\phi(1-\phi) \quad \text{with } D_f \equiv 2|\chi_{AB}|ND_s \quad (8)$$

where D_s is the entropic, self-diffusion coefficient defined in eq 4.

Equation 8 shows that the diffusion coefficient in the enthalpy-driven mixing of polymers is strongly concentration-dependent. In particular, the vanishing of D_M for $\phi = 0$ and $\phi = 1$ leads to very unusual diffusion profiles when either of the polymer pieces brought in contact is initially pure in one of the components:[20] When only one side is pure, the mixing width on that side is finite, with a sharp edge; if both the initial polymer pieces are pure, the width of the mixing region is finite on both sides, and, moreover, the diffusion profile within it is a straight line.

(Of course, as stated above, the simplified form 8 of D_M does not hold when $\phi \to 0$ or $\phi \to 1$, and one has in fact to return to the full expression 7 for which D_M does not exactly vanish... Thus, strictly speaking, the width of the mixing region is never exactly finite, and enthalpic diffusion profiles near $\phi = 0$ and $\phi = 1$ cross over to conventional, infinite "diffusion tails". But this crossover occurs for ϕ or $1 - \phi$ of order $\phi_c = 1/(2|\chi_{AB}|N)$, and in the limit where $|\chi_{AB}|N \gg 1$, ϕ_c is so small that the diffusion tails contain a completely negligible mass of material.)

With this, we conclude our overview on the different aspects of the theory of two-component interdiffusion and come back to the problem of multicomponent interfaces.

3. Description of the Three-Component System and Qualitative Approach

In this section, we present the specific multicomponent system that we chose to study and give some qualitative insight into the structure and dynamics that are expected to emerge. The next section will deal with these issues in a more rigorous way.

As explained in the Introduction, the realm of multispecies system and their interfaces is a very vast one: our aim here is to explore one "model case" among these possibilities, involving three species, and where some interesting features do appear.

3.1. Description of the System and Initial Configuration. We now present the system that we will be concerned with in the rest of this article. The initial ($t = 0$) situation is depicted in Figure 1: the system consists of two pieces of molten polymer which have just been put into contact. The surface of contact (the initial interface) between the pieces is assumed to be planar and is located at position $x = 0$ (the x-axis is drawn perpendicular to the surface of contact). It is assumed that the problem is invariant in the two remaining spatial directions (parallel to the interface).

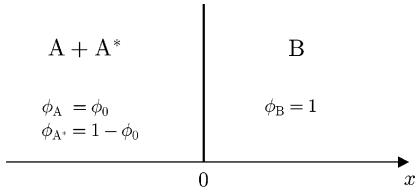

Figure 1. Initial situation of the three-species system. The left-hand side is a blend of two polymers, A and A*, with initial volume fractions $\phi_A = \phi_0$ and $\phi_{A^*} = 1 - \phi_0$. The right-hand side contains only one species, called B, with initial volume fraction $\phi_B = 1$.

The system contains three polymer components which are initially distributed as follows: on the left-hand side, we have a blend of two polymers, A and A*; on the right-hand side, we have a pure polymer, i.e., only one species which is called B. The important step (which is really defining our system) is how to specify the nature of the pairwise affinities between these three components. Our choice is the following: we assume that A and B are attracted to each other (through some specific interaction) and are thus miscible in all proportions; on the contrary, A* and B strongly repel each other and thus have a tendency to form fully segregated phases; and, finally, A and A* are fairly indifferent to each other (i.e., neither attracted or repelled or not much). These features correspond to the following set of Flory parameters:

$$\chi_{AB} < 0, \quad \text{with } |\chi_{AB}|N \gg 1 \quad (9)$$

$$\chi_{A^*B} > 0, \quad \text{with } \chi_{A^*B}N \gg 1 \quad (10)$$

$$\chi_{AA^*} \simeq 0, \quad \text{with } |\chi_{AA^*}|N \ll 1 \quad (11)$$

As we are mainly interested in the effect of the contrast in miscibility between the polymers, and not in chain length effects, it has been assumed above that all polymers have the same polymerization index:

$$N_A = N_{A^*} = N_B = N \quad (12)$$

A three-component system with such features as specified in eqs 9−11 would be quite difficult to realize experimentally, as the above requirements seem at first rather contradictory; they would certainly be achieved only through a fine-tuning of the chemistry of the different polymers involved. We discuss some practical possibilities in the concluding remarks of the article (section 5).

Our choice of system is mainly guided here by the fact that it is one case that leads to the most interesting interfacial structure and dynamics. From the theoretical point of view, this interfacial problem is also original in the sense that, as will be seen shortly, it leads to simultaneous, coupled, entropy- and enthalpy-driven diffusion processes.

3.2. Qualitative Approach to the Multiple Interface Structure. In this section, we present qualitative arguments explaining why, from the initial situation depicted in Figure 1, the interface between the two melts develops a "multiple" structure, i.e., displays several layers or regions of different nature.

Quickly after the onset of contact between the two melts, the interface takes on a configuration as depicted in Figure 2.

As can be seen, the interface is divided in four main zones, labeled I−IV, and the situation can indeed be

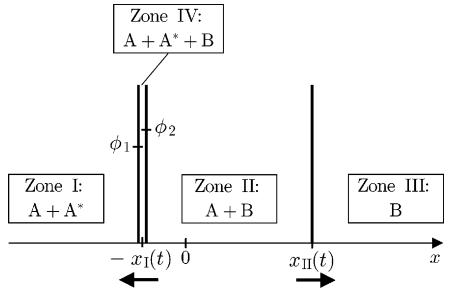

Figure 2. Multiple structure of the interface, with several regions, for $t > 0$. The arrows indicate the direction of motion of the regions' boundaries, $x = -x_I(t)$ and $x = x_{II}(t)$. The quantities ϕ_1 and ϕ_2 indicate the values of the volume fraction in A at the left and right boundaries of region IV.

intuitively understood as explained now. (We do not consider here the transient evolution which takes place in the first instants after contact and leads into the configuration of Figure 2. The interested reader is referred to Appendix A for a more detailed discussion of this transient.)

After the onset of contact, species A and B (which are attracted one to another) start to mix together, thus forming a growing mixing layer (region II) around the initial position ($x = 0$) of the surface of contact between the melts.

On the other hand, A* is repelled by B, and thus, as region II broadens and the A + B mixture spreads, A* must recede toward the left. Thus, region I, which we define as the domain of coexistence of A and A*, is progressively shrinking, with its right boundary moving toward the left.

At the junction between region I (containing A and A*) and region II (containing A and B), there must be a region where all three species coexist (region IV). However, we expect this region IV to be of very small extension as compared to the others, since we know from section 2.1 that strongly immiscible polymers put into contact, like here A* and B, tend to form a very sharp interface with a steep profile; hence, in the remainder of this article, we will neglect the thickness of region IV, and we will not consider any detailed concentration profile within it. It must be emphasized however that region IV, albeit tiny, plays an important role in the dynamics of the system, since all A chains which want to migrate from region I to II must cross region IV (this will be discussed again in the next section).

Finally, there is a last region, III, where B is alone: this comes from the fact that, as explained in section 2.3, when one of the polymer pieces in contact is initially pure (here, $\phi_B = 1$ at $t = 0$ for the piece on the right), enthalpy-driven interdiffusion generates profiles with mixing only over a finite width; thus, there is on the right side of region II a (time-dependent) location where the volume fraction of A reaches zero, and this is what defines the beginning of region III. As the mixing region II broadens, the boundary of region III shifts to the right.

We also introduce in Figure 2 some notations that we will be using intensively in the next sections: $x = -x_I(t)$ gives the position of region IV, and, in our limit where region IV is taken infinitesimally thin, plus or minus exponents ($x = -x_I^{\pm}$) will respectively refer to the right and left boundaries of region IV; $x = x_{II}(t)$ gives the position of the boundary between regions II and III; and $\phi_1(t)$ and $\phi_2(t)$ respectively denote the volume fractions of A just on the left and right of $-x_I$, i.e., $\phi_1 = \phi_A|_{x=-x_I^-}$ and $\phi_2 = \phi_A|_{x=-x_I^+}$.

After having presented an intuitive description of the interfacial structure and dynamics in our system, we will devote the next section to the establishment and solution of the equations governing them.

4. Governing Equations and Results

In this section, we first establish the various equations governing the system (section 4.1) and then solve them numerically (section 4.2). The physical results of our computations are gathered and commented on in section 4.3.

4.1. Governing Equations. From now on, ϕ_A, the volume fraction of A, will be simply denoted by ϕ; i.e., we will use $\phi(x,t) \equiv \phi_A(x,t)$.

Let us start by enumerating our unknowns: these are the locations of the different regions' boundaries ($x = -x_I$ and $x = x_{II}$), the values of the volume fraction in A at $x = -x_I^{\pm}$ (ϕ_1 and ϕ_2), and the time-dependent profile of $\phi(x, t)$ within regions I and II (by definition, $\phi = 0$ within region III). We will thus need a set of six independent equations to determine the solution of the system.

It should be noted that, from the knowledge of ϕ, it is straightforward to retrieve the volume fractions of the other components of the system (using the total volume fraction condition $\phi + \phi_{A^*} + \phi_B = 1$): in region I, where only A and A* are present, one has $\phi_{A^*} = 1 - \phi$ and $\phi_B = 0$; in region II, $\phi_B = 1 - \phi$ and $\phi_{A^*} = 0$; finally, in region III, $\phi_B = 1$ and $\phi = \phi_A = 0$.

We now establish the six independent equations that govern the dynamics of our system.

a. Diffusion Equations. Our first equations simply describe the diffusive motion of polymer A. We must use two different equations, depending on the region considered within the multiple interface.

In region I, A chains diffuse inside an A + A* mixture, with $\chi_{AA^*} \simeq 0$ (eq 11); we are thus in a case of entropy-driven diffusion which is accounted for by eq 3

$$\dot{\phi} - D_s\nabla^2\phi = 0 \quad \text{(region I)} \tag{13}$$

and the initial and boundary conditions are as follows:

$$\phi(t=0) = \phi_0; \quad \phi(x\rightarrow-\infty) = \phi_0; \quad \phi(x = -x_I^-) = \phi_1 \tag{14}$$

In eq 13, the entropic diffusion coefficient D_s is a constant parameter (see eq 4).

In region II, A chains diffuse into an A + B mixture, with $\chi_{AB} < 0$ and $|\chi_{AB}| N \gg 1$ (eq 9); we are there in the presence of an enthalpy-driven diffusion, for which the diffusion coefficient becomes concentration-dependent (see section 2.3). Recalling eq 8, we have

$$D_f = 2|\chi_{AB}|ND_s \quad (D_f \gg D_s) \tag{15}$$

and the diffusion equation in region II can be written as

$$\dot{\phi} - D_f\nabla.(\phi(1-\phi)\nabla\phi) = 0 \quad \text{(region II)} \tag{16}$$

with the initial and boundary conditions (see ref 33)

$$\phi(t=0) = 0; \quad \phi(x=-x_I^-) = \phi_2; \quad \phi(x\rightarrow+\infty) = 0 \tag{17}$$

b. Expansion of the A−B Mixing Region on the Right. Apart from the two diffusion eqs 13 and 16, a third equation can be written, which governs the expansion rate of the mixing region II (A−B mixture) on the right, that is to say, the motion of the boundary $x_{II}(t)$. By definition, $x = x_{II}(t)$ denotes, for any time t, the moving point where the concentration profile ϕ reaches zero (and beyond which only polymer B is present). As shown in the Appendix B to this article, this very definition implies that the *velocity* $\dot{x}_{II}$ of this point has a simple relation to the gradient of ϕ on its left as follows:

$$\dot{x}_{II} = -D_f \nabla\phi|_{x=x_{II}^-} \tag{18}$$

c. Conservation of the A and B Species. We must naturally also take into account equations that ensure the conservation of the different polymer components in the system.

It is shown in Appendix B that the conservation equation for species A leads to the following relation between the velocity $\dot{x}_I$ of the interface of regions I and II and the volume fraction ϕ_1 of A and the gradient $\nabla\phi|_{x=-x_I^-}$ on the left side of it:

$$\dot{x}_I = -\frac{1}{1-\phi_1} D_s \nabla\phi|_{x=-x_I^-} \tag{19}$$

The conservation of the B species, on the other hand, gives a relation between the same velocity $\dot{x}_I$ and the volume fraction and gradient on the right side of this interface:

$$\dot{x}_I = -\phi_2 D_f \nabla\phi|_{x=-x_I^+} \tag{20}$$

Note that the conservation of the third species, A*, follows automatically from the conservation of the two others through the relation between volume fractions $\phi + \phi_{A^*} + \phi_B = 1$ and thus does not bring us a new equation.

d. The Role of Region IV. At this point, we have written down five independent relations; as there are six unknowns, there must be a last physical constraint determining the dynamics of the system. We have so far totally ignored region IV (as defined in Figure 2), where the three species A, A*, and B coexist. As stated earlier, this is because this region is expected to be of very limited extension and, as such, has rightfully been discarded, e.g., from the A and B conservation equations discussed above. However, despite being negligible in mass, region IV must clearly play an essential role regarding the dynamics since all the A material that diffuses from regionI to region II has to transit through it.

Describing precisely the interdependent diffusive process at work within the three-body region IV—solving the "inner problem", in the terms of boundary-layer theory—would undoubtedly represent a complex task and require a study of its own. We rather propose to bypass this difficulty, as we in fact only need very limited information for our purpose: we are only interested in the effect of region IV on the outer dynamics, not in internal details.

We make the simple assumption that region IV opposes no particular resistance to the flow of polymer A passing through it: region IV is "permeable" to A as other regions in the system are, or in other words, the mobility of species A in region IV is not significantly different from the mobility in region I or II. This assumption on mobility appears natural if one considers that although region IV differs from other regions by significant changes in composition (it is the only region where all three species overlap), it does not drastically differ in microscopic structure; hence, the reptational dynamics, which control mobility, should not change significantly within region IV as compared to other regions. (The situation would completely be different if region IV was, for instance, made of a densely cross-linked network which would hinder the passage of polymer chains; one would then rather work under the opposite, "high-resistivity" assumption.)

From this permeability assumption, we can deduce a relation on the chemical potential of species A on each side of region IV: a chemical potential gradient must be present to drive the diffusion of A through region IV, but because this region is both of "low resistivity" and because it is very thin (as argued earlier in the text), the overall drop of chemical potential over region IV will be minute as compared to the potential drop over other (larger) regions and can therefore be completely neglected.

Denoting $\mu_A(-x_I^-)$ the chemical potential of species A just on the left of region IV and $\mu_A(-x_I^+)$ the potential on the right,[34] we thus have

$$\mu_A(-x_I^-) = \mu_A(-x_I^+) \tag{21}$$

As shown in Appendix B, once the expressions of the chemical potentials are written out, this equality between potentials provides our last governing equation in the form of a relation between the volume fractions ϕ_1 and ϕ_2 at the borders of region IV:

$$\phi_1 = \phi_2 \exp[-|\chi_{AB}| N (1-\phi_2)^2] \tag{22}$$

We are now in possession of six independent equations which govern the dynamics in our system and can proceed to solve them.

4.2. Technical Solution. We now present the procedure followed to solve the set of governing equations derived in the previous section (eqs 13, 16, 18, 19, 20, and 22). We will here focus on the technical aspects of the solution, while for the sake of readability, we have grouped together the presentation of the results and their physical content in the next section (section 4.3).

The major difficulty attached to the interdiffusion problem as defined by this set of equations is that it involves two moving boundaries, $x = -x_I(t)$ and $x = x_{II}(t)$: the solution of the diffusion equations in the system requires the application of boundary conditions defined at the moving boundaries, but the motion of the boundaries themselves are directly determined by the diffusive solutions. This self-consistent nature of moving boundary problems make them generally much less straightforward to solve than a conventional diffusion problem; we will here follow the solution scheme described in ref 9.

Our problem falls into the so-called "class A" category,[9] characterized by the fact that the motion of the moving boundaries is uniquely due to the transfer of diffusing substances across them. (This is indeed the meaning of the conservation eqs 38 and 40 discussed in Appendix B.) It is then possible to show that, in a generic fashion, the solution will have the following properties:[9] (i) The concentration of the diffusing species

at the moving boundaries is constant, i.e., ϕ_1 and ϕ_2 are independent of time. (ii) The motion of the moving boundaries is diffusive, i.e., $x_I(t) \sim (D_s t)^{1/2}$ and $x_{II}(t) \sim (D_f t)^{1/2}$.

We build the solution to our problem with the help of these useful results. In accordance with property ii above, we introduce the new quantities a and b defined by

$$x_I(t) = 2a(D_s t)^{1/2} \tag{23}$$

$$x_{II}(t) = 2b(D_f t)^{1/2} \tag{24}$$

The numerical value of a and b will have to be determined as a result of our solution. We also define

$$\epsilon = \frac{D_s}{D_f} = \frac{1}{2|\chi_{AB}|N} \ll 1 \tag{25}$$

which is a small parameter (see eqs 8 and 9).

In the limit where $\epsilon \ll 1$, eq 22 simplifies considerably:

$$\phi_1 = \phi_2 \exp\left(-\frac{(1-\phi_2)^2}{2\epsilon}\right) \xrightarrow{\epsilon \ll 1} 0 \tag{26}$$

Thus, as long as $(1 - \phi_2) \gg \epsilon^{1/2}$ (i.e., as long as ϕ_2 is not too close to unity), we can as well consider that $\phi_1 = 0$ for the rest of our solution to a very good approximation.

We can then immediately solve the diffusion equation (13), valid in region I, along with the boundary conditions (14). The solution can as usual be looked for as a function $\phi(x,t) = f(u)$ of the reduced variable $u = x/2\sqrt{D_s t}$, and from eqs 23 and 26, we see that the boundary condition on the moving boundary simply becomes $\phi(-x_I^-,t) = f(-a) = 0$. Solving the equation on f, we finally find the following concentration profile in region I, which involves the error function erf $u = (2/\sqrt{\pi})\int_0^u e^{-u^2}\,du$, classical for semiinfinite media:

$$\phi(x,t) = \phi_0 - \frac{\phi_0}{1 - \mathrm{erf}\, a}\left[1 + \mathrm{erf}\left(\frac{x}{2\sqrt{D_s t}}\right)\right] \quad \text{(region I)} \tag{27}$$

We next turn to the determination of a and thus to the determination of the position of the moving boundary at $x = -x_I$. Equation 19 will serve this purpose: with $\phi_1 = 0$, it simplifies to $\dot{x}_I = -D_s \nabla\phi|_{x=-x_I^-}$. Then, with the help of eq 23, which yields $\dot{x}_I = a(D_s/t)^{1/2}$ and of eq 27 which yields an expression of $\nabla\phi|_{x=-x_I^-}$, eq 19 finally brings the relation

$$\sqrt{\pi} a e^{a^2}(1 - \mathrm{erf}\, a) = \phi_0 \tag{28}$$

This equation on a can be solved numerically to give the value of a as a function of the fundamental parameter ϕ_0 (which describes the initial state of the system). The result of the numerical solution is shown in Figure 7.

The next step is to solve the diffusion equation (16) under the conditions (17) to find the concentration profile in region II. As eq 16 is a nonlinear equation without analytical solution (to the best of our knowledge), we will resort to numerical integration. We here again look for a solution $\phi(x,t) = g(v)$ of the (new) reduced variable $v = x/2\sqrt{D_f t}$. The resulting differential equation on g turns out as

$$\frac{d}{dv}\left(g(1-g)\frac{dg}{dv}\right) = -2v\frac{dg}{dv} \tag{29}$$

and the boundary conditions of eq 17 translate to

$$\text{(i) } \phi|_{x=-x_I^+} = g|_{v=-a\sqrt{\epsilon}} = \phi_2, \quad \text{(ii) } \phi|_{x\to+\infty} = g|_{v\to+\infty} = 0 \tag{30}$$

It has to be noted that these boundary conditions, as such, are not sufficient to directly proceed to numerical integration because the quantity ϕ_2 appearing there is also an unknown. We thus need a supplementary condition, which will be provided by the conservation equation of the B species (eq 20): using the definition of a (eq 23) and the definition of the reduced variable v, eq 20 can be rewritten as

$$\frac{dg}{dv}|_{v=-a\sqrt{\epsilon}} = -\frac{2a\sqrt{\epsilon}}{\phi_2} \tag{31}$$

We have now enough equations to compute $g(v)$ and the associated concentration profile in region II. We solve the set of eqs 29−31 by a trial-and-error procedure: we choose an arbitrary value for the unknown ϕ_2; based on the corresponding initial conditions provided by eqs 30-(i) and 31, a numerical integration of eq 29 is performed; the obtained solution g is then evaluated at infinity, and its value is compared to zero (eq 30-(ii)); if different, the whole numerical procedure is resumed with a new chosen value for ϕ_2, until the correct value of ϕ_2, satisfying eq 30-(ii), is found. At the end of this process, we eventually obtain the actual profile of concentration $\phi(x,t) = g(v)$ in region II along with the value of ϕ_2 in our system. (See further down for results.)

We are at this point in possession of the profiles $\phi(x,t)$ in regions I−III as well as of the numerical values of a, ϕ_1, and ϕ_2. To complete our solution, we still need to find the value of b, which is related to the position of the border between regions II and III. This is easily performed numerically: by transposing the equation of motion for established earlier (eq 18) in terms of the self-similar function $g(v)$ and applying the definition of b (eq 24), one obtains the relation

$$-2b = \frac{dg}{dv}|_{v=b} \tag{32}$$

i.e., b is a quantity such that the slope of g at $v = b$ is equal to twice the value of b (with changed sign). The search for such a b can be carried on numerically with the function g calculated previously: the graph of b as a function of ϕ_0 can be found in Figure 7.

4.3. Presentation of the Results. We now present and comment on the results of the model, as obtained through the procedure described in the previous section.

As seen in eqs 23 and 24, the different "compartments" or layers composing the multiple interface are separated by diffusive fronts: $x = -x_I(t) = -2a(D_s t)^{1/2}$ and $x = x_{II}(t) = 2b(D_f t)^{1/2}$, with a and b are numerical parameters (see below for their values). The evolution in time of the concentration profiles of the different components is thus self-similar, and for this reason, it is useful to present them here in terms of the reduced variable $u = x/2(D_s t)^{1/2}$.

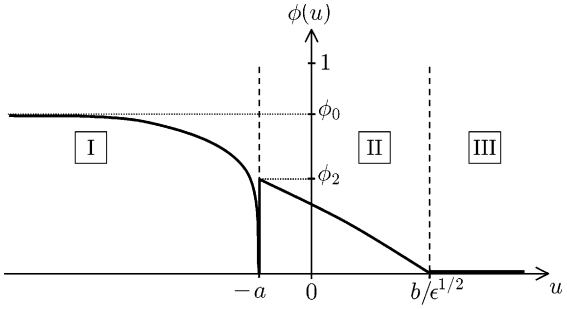

Figure 3. Sketch of the generic self-similar diffusion profile for species A: the volume fraction ϕ has been drawn vs the reduced variable $u = x/2\sqrt{D_s t}$. The volume fractions used in the text, ϕ_0 and ϕ_2, are also represented. In domain I (i.e., for $u < -a$), the concentration profile is an error function; in domain II (i.e., for $-a < u < b/\epsilon^{1/2}$), the profile is quasi-linear. In region III, A is absent.

We remind our reader that there are two main physical parameters to our solution: ϕ_0, which represents the content in A of the initial A + A* blend, and the small parameter $\epsilon = 1/(2|\chi_{AB}|N) \ll 1$, which is related to the strength of the attraction between A and B chains and the polymer chain length.

As these parameters were varied over a wide range of values (ϕ_0 between 0.1 and 0.9, ϵ between 10^{-5} and 0.1), it was observed that, remarkably enough, the (self-similar) diffusion profiles obtained retain the same aspect throughout; the main effect of varying the parameters is simply to rescale one or the other of the characteristic dimensions of the self-similar solution (i.e., stretch or shrink it in some region).

This generic self-similar diffusion profile for the A species is sketched in Figure 3 in terms of the reduced variable u. The fronts $x = -x_I(t)$ and $x = x_{II}(t)$ are respectively located at $u = -a$ and $u = b/\sqrt{\epsilon}$. Starting from the left in Figure 3, the profile in region I is given by an "error function", typical of diffusion problems, and drops to zero at the approach of region II (since we proved that $\phi_1 \simeq 0$ in most practical cases). At the boundary between regions I and II (we neglect the thickness of the intermediate region IV), there is a discontinuous concentration jump from $\phi = 0$ to $\phi = \phi_2$, and then the diffusion profile decreases smoothly until reaching zero again at the border with region III. It should be emphasized as a very interesting feature of the solution that the amplitude ϕ_2 of this concentration jump remains constant in time and does not die away during the diffusion process.

Another interesting feature is the depletion near $u = -a$ of species A ($\phi \to 0$). The depletion is a direct reflection of the fact that it is energetically much more favorable for A to be in the A + B blend of region II ($\chi_{AB} < 0$) than in the A + A* blend of region I ($\chi_{AA^*} \simeq 0$); therefore, as time passes, region II continuously sucks A chains out of region I, creating in the latter a depleted zone which grows with time (as $\sqrt{D_s t}$).

We also note that, from an empirical point of view, the profile in region II does not have a very significant curvature; if needed, we may thus approximately regard it as a straight line.

As an illustration of the generic sketch of the diffusion profile described above, we have plotted in Figure 4 two actual profiles, computed numerically for different values of ϕ_0 (and same ϵ), which do show that, within some rescaling, the generic shape of Figure 3 is retained in both cases.

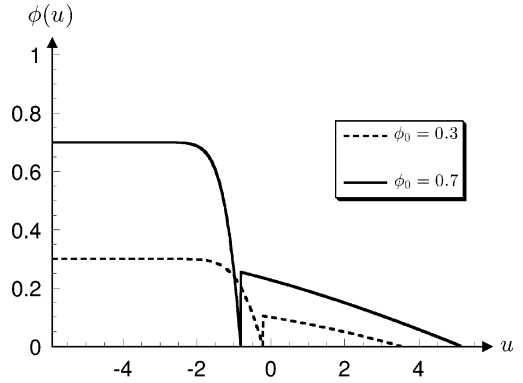

Figure 4. Numerical profiles for the volume fraction $\phi(u)$ of the A species (with $u = x/2\sqrt{D_s t}$). The chain length and Flory parameter are $N = 10^3$ and $\chi_{AB} = 0.1$, yielding $\epsilon = 5 \times 10^{-3}$. The solution $\phi(u)$ has been represented for two values of the initial volume fraction of the A species in the A−A* blend: $\phi_0 = 0.3$ and $\phi_0 = 0.7$.

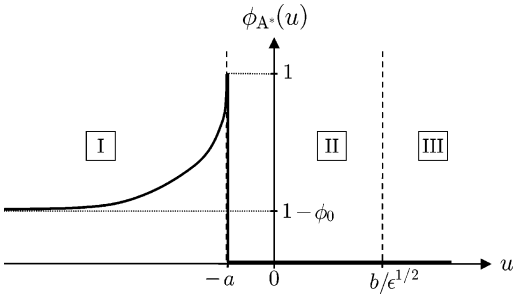

Figure 5. Sketch of the generic self-similar diffusion profile for the A* species: the volume fraction ϕ_{A^*} has been drawn vs the reduced variable $u = x/2\sqrt{D_s t}$. In region I, $\phi_{A^*} = 1 - \phi$ and is thus given by a complementary error function. In the other regions, A* is absent.

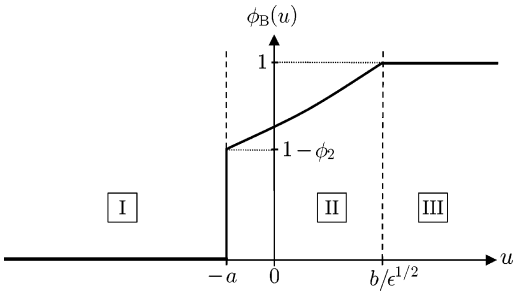

Figure 6. Sketch of the generic self-similar diffusion profile for the B species: the volume fraction ϕ_B has been drawn vs the reduced variable $u = x/2\sqrt{D_s t}$. In region I, B is absent; in region II, the profile of B is the complement of A ($\phi_B + \phi = 1$) and is quasi-linear; in region III, B is alone.

For completeness, we also give the corresponding generic self-similar profiles for the other mixture components in Figures 5 and 6. As reminded in Figure 3, the diffusion profiles involves several characteristic quantities a, b, and ϕ_2, whose values we now consider in detail.

In Figures 7 and 8, we plot the variations of these quantities as functions of our parameter ϕ_0, i.e., $a(\phi_0)$, $b(\phi_0)$, and $\phi_2(\phi_0)$, at fixed ϵ (i.e., we work at given system chemistry and change the initial composition of the system). It is observed that these quantities show a steady increase with ϕ_0. Results are presented for the range $0.1 \lesssim \phi_0 \lesssim 0.9$, which should cover most practical cases; see ref 35 about situations where $\phi_0 \to 0$ or $\phi_0 \to 1$.

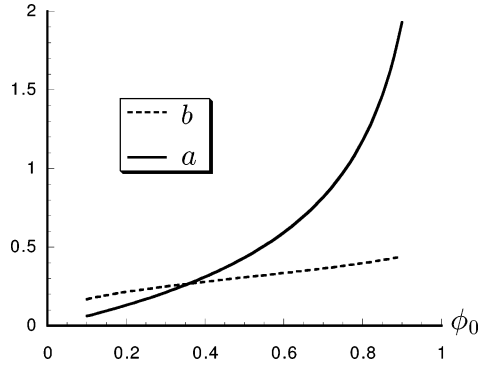

Figure 7. Values of the numerical factors a and b, which characterize the two moving boundaries $x_I(t) = -2a(D_s t)^{1/2}$ and $x_{II}(t) = 2b(D_f t)^{1/2}$, plotted vs the initial volume fraction ϕ_0. (ϕ_0 is ranging from 0.1 to 0.9 and ϵ is fixed at 5×10^{-3}.)

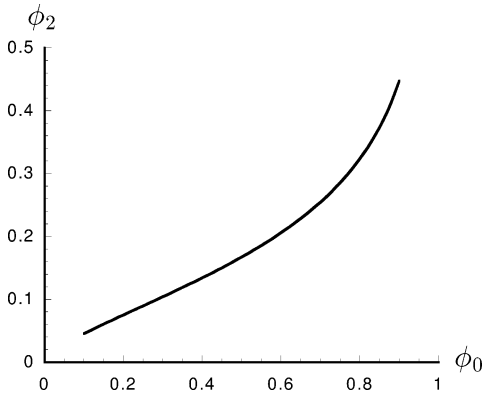

Figure 8. Plot of the quantity ϕ_2, which corresponds to the amplitude of the concentration jump at the border between region I and II, vs the parameter ϕ_0. (ϕ_0 is ranging from 0.1 to 0.9 and ϵ is fixed at 5×10^{-3}.)

It is also possible to give rough analytical estimates of the dependence of a, b, and ϕ_2 with respect to our other main parameter, ϵ. The quantity a is given by the solution of eq 28, which involves only ϕ_0; thus we see that a has no functional dependence on ϵ (at least in the regime $\epsilon \ll 1$ considered in this article). Let us now estimate the dependencies of ϕ_2 and b on ϵ: for that purpose, we will consider, in first approximation, that the concentration profile is linear in region II (see above). Writing as previously the solution $\phi(x,t) = g(v)$ in terms of the reduced variable $v = x/2(D_s t)^{1/2}$, the ("constant") value of the slope dg/dv is easily estimated: since $g(v)$ goes from ϕ_2 at the left boundary of region II ($v = -a\sqrt{\epsilon}$) to zero at the right boundary ($v = b$), we have dg/d$v \simeq -\phi_2/(b + a\sqrt{\epsilon}) \simeq -\phi_2/b$. We then use this expression of the slope into eq 30-(i) and eq 31 and solve this set of two equations for b and ϕ_2. This brings the following estimates:

$$b \simeq \left(\frac{a^2}{4}\epsilon\right)^{1/6}, \quad \phi_2 \simeq (2a^2\epsilon)^{1/3} \tag{33}$$

In terms of scaling laws with respect to ϵ, we thus have

$$b \sim \epsilon^{1/6}, \quad \phi_2 \sim \epsilon^{1/3}, \quad a \sim \epsilon^0 \tag{34}$$

where the last equation is meant to recall that a has no dependence on ϵ.

Finally, we conclude the presentation of our results by emphasizing one unusual and notable feature of our solution: as time goes on, region II, where A and B mix, grows in a very asymmetric fashion, relative to the position of the initial interface ($x = 0$ at $t = 0$); this is due to the fact that its two boundaries are of very different nature, with the right boundary $x = x_{II}$ having a much faster diffusive motion than the left boundary $x = -x_I$ (because $D_f \gg D_s$). The ratio of these two boundaries' position is in fact independent of time and can be estimated as

$$\frac{x_I(t)}{x_{II}(t)} = \frac{a}{b}\left(\frac{D_s}{D_f}\right)^{1/2} \sim \epsilon^{-1/6}\epsilon^{1/2} \sim \epsilon^{1/3} \tag{35}$$

The sluggishness of the motion of x_I relative to x_{II} thus becomes more pronounced as ϵ becomes smaller, i.e., if the attraction between A and B is made stronger or if the polymer chains length is increased (see eq 25).

We have now completed the solution of the dynamics of our three-species system and have presented the results that were obtained.

5. Concluding Remarks

In this article, we studied the evolution of the interface between two polymer melts, in a specific case where three species of strongly contrasting chemical affinities were involved. It was found that, due to the simultaneous presence of entropy- and enthalpy-driven diffusion processes, the dynamics at the interface is unusual (with a very asymmetric growth of the mixing layer) and that, moreover, the interface shows a peculiar spatial structuration in three distinct layers of different chemical compositions.

Let us now close with some remarks. Obtaining a triad of polymers with chemical properties such as specified in eqs 9−11 is certainly a difficult task. One potential way could be the following: (i) having A and B strongly attracted to each other through the existence of hydrogen bonds, (ii) having A* a very slightly modified variant of A, where hydrogen bonding to B becomes unavailable; then between A and B, van der Waals attractions will dominate, leading to repulsion, while hopefully A and A* will remain similar enough and roughly indifferent to each other. Another, powerful way of achieving such a system may also be through the use of copolymers.

The specific case which has been described and studied in this article is, as has been argued in the Introduction, only one limiting situation in a vast range of multiple species interfaces in polymer systems and has been selected for the strong opposing tendencies in the chemical affinities of the involved polymers. Our hope is however to demonstrate on this example the richness of multiple-species interfaces, where many other such "selected cases" would be worth investigating and studying for their peculiar structure and dynamics.

A related, though different, problem to that of two multicomponent melts facing each other is the situation of a melt facing a loosely cross-linked gel (this perspective was suggested to us by one of the referees). In the example studied in this article, an A + A* blend would be brought into contact with a gel of B. The subsequent evolution might develop interesting features: the motion of the $x_{II}(t)$ front (as defined on Figure 2) would describe the imbibition of the B gel by the A species, while the displacement of the $x_I(t)$ border would be dictated by the swelling of the gel—this would imply the

inclusion of new elastic terms in the model's equations. We note however that, in practice, the dynamics of polymer diffusion into a network can prove very subtle, with a predominant role of preexisting heterogeneities (e.g., in cross-link density) within the network.[36]

From the application point of view, the ability to spontaneously form (at least in some cases) a multilayered interface between two polymer pieces might lead to interesting perspectives in the design of multilayer polymer films[37]—which are widely used for product packaging, for instance. Whereas conventional technology includes processes like coating, lamination, or coextrusion to form multilayered films, here the layering appears by means of a purely diffusional process. The chemical composition and the spatial organization of the layering could be controlled through an appropriate choice of chemical affinities between the different species in interaction, and once the desired result is attained (e.g., prescribed layer thicknesses), the system could be quenched to freeze the diffusion process.

Acknowledgment. We are very grateful to F. Brochard-Wyart, F. Chevy, C. Creton, and M. Winnik for useful discussions. We also thank our anonymous reviewers for several deep comments which led to improvements in the article. A.A. acknowledges the support of EPSRC (UK) through a Post-doctoral Fellowship in Theoretical Physics (GR/R95098).

Appendix A. Transient Behavior at the Onset of Contact

In this Appendix, we discuss the transient behavior taking place in the first instants after the contact between the initial melts is established and how it leads to the layered configuration depicted in Figure 2 of the main text.

Let us consider the situation immediately after the onset of contact (see Figure 1) from the point of view of species B: because of thermal agitation, a few B molecules start to extend chain portions into the A + A* blend, of respective volume fractions ϕ_A and $\phi_{A^*} = 1 - \phi_A$. These first B chain portions will then experience an A + A* environment with an average, "effective" Flory parameter

$$\bar{\chi}_B \simeq \phi_A \chi_{AB} + \phi_{A^*} \chi_{A^*B} \tag{36}$$

(in a mean-field picture). Given the opposite signs of χ_{AB} and χ_{A^*B}, this effective $\bar{\chi}_B$ may be positive or negative depending on the composition of the A + A* blend. Defining

$$\phi_c = \chi_{A^*B}/(\chi_{AB} + |\chi_{A^*B}|) \tag{37}$$

we have two cases depending on the initial ($t = 0$) content $\phi_A = \phi_0$ in A of the A + A* blend: either $\phi_0 < \phi_c$ or $\phi_0 > \phi_c$. We discuss below the two scenarios that ensue for the transient evolution of the system at short times.

If the initial situation is such that $\phi_0 < \phi_c$, we see from eq 36 that $\bar{\chi}_B > 0$, which means that the environment seen by the B chains exploring the initial A + A* blend is enthalpically unfavorable. Therefore, the triple region A + A* + B created by this diffusion remains of very small extension and corresponds to our region IV in Figure 2. On the other hand, the diffusion of species A into the B melt is very favorable ($\chi_{AB} < 0$), and thus A molecules do at the same time migrate from the initial A + A* blend through the triple region IV and create a mixing layer A + B as seen in Figure 2. At that point in time, the layered structure of the interface is established, and the subsequent dynamics of the system crosses over to that described in the main text (see section 3.2).

Alternatively, if the initial situation of the system is such that $\phi_0 > \phi_c$, eq 36 tells us that $\bar{\chi}_B < 0$, and in that case, the environment seen by the B molecules initially in contact with the A + A* blend is favorable. Therefore, it is expected that after the onset of contact B molecules will start diffusing into the A + A* blend, and thus a growing region where the three species A, A*, and B overlap will form. This may at first seem at odds with the layered configuration of Figure 2 and especially with the assumption of a thin triple region invoked in the main text. However, if one considers the point of view of species A and A*, simple energetic arguments make it clear that the initial growth of the triple region will be short-lived: first, the triple region makes an unfavorable environment for A* (the local effective Flory parameter for A*, as an average of $\chi_{AA^*} \simeq 0$ and $\chi_{A^*B} > 0$, is always positive), and thus A* will demix and migrate back to the A + A* melt on the left; second, rather than staying within the triple region where part of their contacts are made with A* molecules (with no enthalpy gain), A chains will seek to augment favorable $\chi_{AB} < 0$ contacts and will thus preferably migrate into the pure B region on the right of the triple region—thereby creating the A + B region described in the main text as region II. As both these processes occur at the expense of the triple region, the size of the latter can only remain modest. Qualitatively at least, it thus becomes apparent that, here again, the system rapidly evolves to the configuration of Figure 2. A more precise description of the transient dynamics just sketched would nevertheless be desirable and remains ahead of us.

(Note: in the limit where the initial A + A* blend is in fact almost purely composed of A, i.e., ϕ_0 very close to unity, we expect some of the above arguments to break down; the system will not form layers at the interface but should simply evolve as in the known situation of a pure melt of A in contact with a pure melt of B.[20])

Appendix B. Derivation of Governing Equations

In this Appendix, we give a detailed derivation of some of the governing equations presented in section 4.1.

Equation of Motion for $\chi_{II}(t)$. Equation 18 is obtained as follows. By definition, $x_{II}(t)$ is the point such that, at any time t, $\phi(x_{II}(t),t) = 0$. Since ϕ is a constant over time at that point, we also have that the total time derivative at that (moving) point, $d\phi/dt|_{x=x_{II}}$, must be zero:

$$\frac{d\phi}{dt}|_{x=x_{II}} = \dot{\phi}|_{x=x_{II}} + \dot{x}_{II} \nabla\phi|_{x=x_{II}} = 0$$

Furthermore, using the diffusion eq 16 and $\phi|_{x=x_{II}} = 0$, another expression for $\dot{\phi}$ is easily obtained:

$$\dot{\phi}|_{x=x_{II}} = D_f (\nabla\phi|_{x=x_{II}})^2$$

Substitution of the latter equation into the former yields eq 18.

Conservation of the B Species. We now show how relation 20 results from the conservation of the B species.

As a little reflection from the consideration of Figures 1 and 2 can make clear, the conservation of the B species reads as follows:

$$\int_{-x_{\mathrm{I}}(t)}^{x_{\mathrm{II}}(t)} \phi_{\mathrm{B}}\, \mathrm{d}x = x_{\mathrm{II}}(t)\cdot 1 \tag{38}$$

This expression simply states that, when considering the situation at a certain time $t > 0$, all the initial B material which was comprised between $x = 0$ and the present position $x = x_{\mathrm{II}}(t)$ (a quantity equal to $x_{\mathrm{II}}\cdot 1$ since the initial volume fraction of B was one) has been redistributed by virtue of the interdiffusion process all over region II (hence the term $\int_{-x_{\mathrm{I}}}^{x_{\mathrm{II}}} \phi_{\mathrm{B}}\, \mathrm{d}x$ on the left-hand side). Using $\phi_{\mathrm{B}} = 1 - \phi$, one then obtains

$$\int_{-x_{\mathrm{I}}(t)}^{x_{\mathrm{II}}(t)} \phi\, \mathrm{d}x = x_{\mathrm{I}}(t) \tag{39}$$

Differentiating eq 39 once with respect to time, using eq 16 and $\phi(x_{\mathrm{II}}) \equiv 0$, one obtains a local version of this integral equation: $\dot{x}_{\mathrm{I}} = -\phi_2 D_{\mathrm{f}} \nabla\phi|_{x=-x_{\mathrm{I}}^+}$, which is exactly eq 20.

Conservation of the A Species. We now derive eq 19 from the conservation of species A. The conservation equation for A has the form

$$\int_{-x_{\mathrm{I}}(t)}^{x_{\mathrm{II}}(t)} \phi\, \mathrm{d}x = \phi_0 x_{\mathrm{I}}(t) + \int_{-\infty}^{-x_{\mathrm{II}}(t)} (\phi_0 - \phi)\, \mathrm{d}x \tag{40}$$

This expression has the following meaning: at time t, the A material enclosed in region II ($\int_{x=-x_{\mathrm{I}}}^{x=x_{\mathrm{II}}} \phi\, \mathrm{d}x$) comes from the material which was initially present between $x = -x_{\mathrm{I}}$ and $x = 0$ at volume fraction ϕ_0, plus the amount that has diffused from region I ($\int_{-\infty}^{-x_{\mathrm{II}}} (\phi_0 - \phi)\, \mathrm{d}x$). Using eq 39 into eq 40, then differentiating with time and substituting with the diffusion eq 13, one finally obtains the following local version for the conservation of the A species: $\dot{x}_{\mathrm{I}} = -(1 - \phi_1)^{-1} D_{\mathrm{s}} \nabla\phi|_{x=-x_{\mathrm{I}}^-}$, which is precisely eq 19.

Relation between ϕ_1 and ϕ_2. We now explain how one obtains eq 22 from eq 21.

Using classical formulas[1,5,38] to compute the chemical potential of A, one obtains the expression

$$\mu_{\mathrm{A}} = kT[\log \phi + \chi N(1 - \phi)^2] \tag{41}$$

This expression for holds for blends made of two polymer species, characterized by a Flory parameter χ (and under the assumption that these species have the same chain length N). Thus, eq 41 should not be used to compute μ_{A} within region IV, where three components coexist, but it can indeed be used at the border with region I on the left and at the border with region II on the right—there one of the components drops to zero concentration, thereby leaving us with two species only (see also ref 34).

On the left border of region IV ($x = -x_{\mathrm{I}}^-$), we only have the two species A and A* (since $\phi_{\mathrm{B}} \to 0$), and accordingly, we can apply formula 41 with $\chi = \chi_{\mathrm{AA}^*} \simeq 0$, which yields

$$\frac{\mu_{\mathrm{A}}(-x_{\mathrm{I}}^-)}{kT} = \log \phi_1$$

Similarly, on the right border ($x = -x_{\mathrm{I}}^+$), only A and B coexist, and we find

$$\frac{\mu_{\mathrm{A}}(-x_{\mathrm{I}}^+)}{kT} = \log \phi_2 + \chi_{\mathrm{AB}} N(1 - \phi_2)^2$$

Writing the equality between the above two expressions of the chemical potential (as required by eq 21) yields the governing eq 22.

References and Notes

(1) Jones, R. A. L.; Richards, R. W. *Polymers at Surfaces and Interfaces*; Cambridge University Press: Cambridge, 1999.
(2) Wool, R. P. *Polymer Interfaces: Structure and Strength*; Hanser Publications: Cincinnati, 1995.
(3) *Physics of Polymer Surfaces and Interfaces*; Sanchez, I. C., Fitzpatrick, L. E., Eds.; Butterworth-Heinemann: London, 1992.
(4) *Polymer Surfaces and Interfaces III*; Richards, R. W., Peace, S. K., Eds.; Wiley and Sons: New York, 1999.
(5) de Gennes, P.-G. *Scaling Concepts in Polymer Physics*; Cornell University Press: Ithaca, 1979.
(6) The free energy of mixing of an A/B polymer melt is rather well described by the simple Flory−Huggins approach, which is a tractable, two-species polymeric version of a lattice gas model. The two first terms on the right-hand side of expression 6 give the entropic contribution of f, which is assumed to take a simple ideal gas form. The last term stands for the enthalpy of mixing, estimated within a mean-field picture. See: (a) Flory, P. *Principles of Polymer Chemistry*; Cornell University Press: Ithaca, 1971. (b) Doi, M. *Introduction to Polymer Physics*; Oxford University Press: Oxford, 1996. (c) Huggins, M. *J. Am. Chem. Soc.* **1942**, *64*, 1712.
(7) Bates, F. S.; Wignall, G. D. *Phys. Rev. Lett.* **1986**, *57*, 1429.
(8) (a) Helfand, E. *Polymer Compatibility and Incompatibility*; K. Solc. Chur: Harwood, 1982. (b) Helfand, E.; Tagami, Y. *J. Polym. Sci.* **1971**, *B9*, 741. (c) Helfand, E.; Tagami, Y. *J. Chem. Phys.* **1971**, *56*, 3592. (d) Helfand, E.; Tagami, Y. *J. Chem. Phys.* **1972**, *57*, 1812.
(9) Crank, J. *The Mathematics of Diffusion*; Clarendon Press: Oxford, 1975.
(10) de Gennes, P.-G. *C. R. Acad. Sci. Paris Ser. II* **1980**, *291*, 219.
(11) Prager, S.; Tirell, M. *J. Chem. Phys.* **1981**, *75*, 5194.
(12) Kim, Y. H.; Wool, R. P. *Macromolecules* **1983**, *16*, 1115.
(13) Adolf, D.; Tirell, M.; Prager, S. *J. Polym. Sci., Polym. Phys. Ed.* **1985**, *23*, 413.
(14) Zhang, H.; Wool, R. P. *Macromolecules* **1989**, *22*, 3018.
(15) Brochard, F.; de Gennes, P.-G. *Europhys. Lett.* **1986**, *1*, 221.
(16) Brochard-Wyart, F.; de Gennes, P.-G. *Makromol. Chem. Macromol. Symp.* **1990**, *40*, 167.
(17) Shibayama, M.; Yang, H.; Stein, R. S.; Han, C. C. *Macromolecules* **1985**, *18*, 2179.
(18) (a) Onsager, L. *Ann. N.Y. Acad. Sci.* **1933**, *34*, 241. (b) Onsager, L. *Phys. Rev.* **1931**, *37*, 405.
(19) de Gennes, P.-G. *J. Chem. Phys.* **1980**, *72*, 4756.
(20) Brochard, F.; Jouffroy, J.; Levinson, P. *Macromolecules* **1983**, *16*, 1638.
(21) Brochard, F.; Jouffroy, J.; Levinson, P. *J. Phys., Lett.* **1983**, *44*, 455.
(22) Kramer, E. J.; Green, P.; Palstrøm, C. J. *Polymer* **1984**, *25*, 473.
(23) Sillescu, H. *Makromol. Chem. Rapid Commun.* **1987**, *8*, 393.
(24) Jabbari, E.; Peppas, N. A. *Polymer* **1995**, *36*, 575.
(25) (a) Akcasu, A. Z. *Macromol. Theory Simul.* **1997**, *6*, 679. (b) Akcasu, A. Z.; Nägele, G.; Klein, R. *Macromolecules* **1995**, *28*, 6680.
(26) (a) Klein, J. *Nature (London)* **1978**, *271*, 143. (b) Klein, J.; Briscoe, B. J. *Proc. R. Soc. London A* **1979**, *365*, 53.
(27) Gilmore, P. T.; Falabella, R.; Lawrence, R. L. *Macromolecules* **1980**, *13*, 880.
(28) Jordan, E. A.; Ball, R. C.; Donald, A. M.; Fettes, L. J.; Jones, R. A. L.; Klein, J. *Macromolecules* **1988**, *21*, 235.
(29) Seggern, J. V.; Klotz, S.; Cantow, H. J. *Macromolecules* **1989**, *22*, 3828.

(30) Meier, G.; Fytas, G.; Momper, B.; Fleicher, G. *Macromolecules* **1993**, *26*, 5310.
(31) (a) Brochard-Wyart, F. *C. R. Acad. Sci. Paris Ser. II* **1987**, *305*, 657. (b) Brochard-Wyart, F. *Stud. Polym. Sci.* **1988**, *2*, 249.
(32) In the regime of entangled polymer chains, Brochard's amended approach gives exactly the same expressions for the diffusion coefficients as in the model of Kramer et al. It should be noted, however, that a discrepancy remains in the case of short, nonentangled chains.
(33) Note that the last boundary condition in eq 17 resides within region III, not II; this is admissible because the diffusion equation (16) is indeed valid in region III as well as in region II. The boundary conditions stated here in fact automatically generate a solution which vanishes to zero at some finite position $x = x_{II}(t)$ and afterward keeps that value for all $x > x_{II}$: they thereby naturally give birth to our region III (defined earlier as the region where $\phi = 0$) without the need of further constraints to be imposed and are the correct ones to use.
(34) If conditions are such that region IV is so thin as to be comparable to the radius of gyration of the chains, chemical potentials cannot be defined within this region (because nonlocal, square-gradient terms enter into the system's free energy). In that case, the chemical potentials appearing in equality 21, which are calculated "at the left and right boundaries" of region IV, should naturally be understood as evaluated slightly away from those boundaries (typically a few radii of gyration), where their definition makes sense again.
(35) Results in the main text are presented for initial fractions ϕ_0 of the A species comprised between 0.1 and 0.9 which cover most of the interesting situations. Outside this range, some of the assumptions used in the solution of the model do break down; however, the physical situation is simple since it is basically getting back to usual two-species configurations (as described in the overview, section 2), with no "interfacial layering" at all. For the smaller fractions ($\phi_0 \rightarrow 0$), the system tends to the situation of an (almost) pure melt of A* facing a B melt (with a sharp A*/B interface in between). For the higher initial fractions ($\phi_0 \rightarrow 1$), the evolution is on the contrary that of an (almost) pure A melt facing a pure B melt, with enthalpic mixing taking place.
(36) Russ, T.; Brenn, R.; Abel, F.; Boué, F.; Geoghegan, M. *Eur. Phys. J. E* **2001**, *4*, 419.
(37) Briston, J. H. In *Encyclopedia of Advanced Materials*; Bloor, D., Brook, R. J., Flemings, M. C., Mahajan, S., Eds.; Pergamon Press: New York, 1994.
(38) Doi, M. *Introduction to Polymer Physics*; Oxford University Press: Oxford, 1996.

MA0356008